POLYGONAL MIRROR LASER SCANNING HEADS: CHARACTERISTIC FUNCTIONS

Virgil-Florin DUMA[1,2]

[1] 3OM Optomechatronics Group, *Aurel Vlaicu* University of Arad, Arad 310130, Romania
[2] Polytechnic University of Timisoara, Doctoral School, Timisoara 300222, Romania
E-mail: duma.virgil@osamember.org

Abstract. The study analyzes Polygonal Mirror (PM) scanning heads for one of their most utilized setups: with an off-axis PM and the incident parallel laser beam orthogonal to the optical axis of the objective lens. The study places under the umbrella of the same theory systems that range from PMs with a small number of facets (e.g., industrial measurements) to PMs with a large number of facets - as for high-end biomedical imaging systems, in particular for swept sources utilized in Optical Coherence Tomography (OCT). The characteristic functions of PM heads are derived: scanning function and velocity, pairs of rotational angles, and duty cycle. Two migration functions are also obtained, to characterize the displacement of the object point of the lens, as produced by the beam movement on the PM facet. Each function is studied with regard to the parameters of the PM head: number of facets, inner radius, rotational speed, eccentricity of the incident laser beam with regard to the PM pivot, as well as the distance from the beam to the lens. The theoretical results are validated experimentally. Considerations on the design of PM scanning heads are extracted from the analysis.

Key words: laser scanners, polygon mirrors, geometrical optics, multi-parametric analysis, swept sources, optical coherence tomography.

1. INTRODUCTION

Laser scanners have a wide area of applications [1, 2], from commercial and industrial (e.g., for dimensional measurements, laser manufacturing, or 3D printing) to high-end applications like biomedical imaging. The latter include rapidly evolving domains like Optical Coherence Tomography (OCT) [3, 4] or more classical ones, like Confocal Microscopy, as well as combinations of different techniques [5].

From the variety of laser scanners that have been developed [1], several types are in use: oscillatory (galvanometer or resonant, the latter built especially as Micro-Electro-Mechanical Systems (MEMS) [6]), with rotating mirrors (plane, polygonal, or pyramidal), refractive, electro-, and acousto-optical [1, 2]. While Galvanometer Scanners (GSs) have imposed themselves because of their good overall parameters (i.e., precision, scan frequency (f_s) and amplitude, and cost per scan axis) in compact constructs [7], other types of scanners have niche applications that take advantage of their superior capabilities in certain respects [8]. Especially Polygonal Mirror (PM) scanners had a strong comeback for applications that require high scan speeds, such as laser sources scanned in frequency for Swept Source (SS) OCT [9–12], technique that has proven advantages with regard to other OCT modalities [3]. In this respect GSs have the major drawback of the non-linear stop-and-turn portions of the oscillatory movement of their mirror; therefore, galvoscanning regimes have to be optimized to increase their duty cycle (i.e., the time efficiency of the scanning process) [13] and to correct distortions, for example in OCT images [14, 15]. In contrast to GSs, which usually operate with f_s of up to 1kHz and bi-directional scan, rotational PM scanners perform fast, uni-directional scan with a f_s given by the PM angular speed ω and by its number of facets (n). Nowadays motors reach a ω of 60 krpm (while motors with 120 krpm are developed) and n ranges between 5 (for commercial PMs) [16] to 24 [17] and up to 128 for SSs [9], while PMs with 72 facets are usual [10]; therefore values of f_s in excess of 100 kHz are reachable. Other advantages of PMs refer to their large throughput, aperture, and scan angles.

Therefore, besides classical scanners applications [2, 16], a variety of systems take advantage of these unique features of PMs, including: (i) telescope [9, 10] and telescope-less SSs for OCT – the latter in Littrow [11] or Littman [12] configurations; (ii) scanning delay line setups for Fourier Domain OCT [17]; (iii) bi-

dimensional (2D) PM plus GS devices, where the PM produces fast scan lines that are precisely positioned by the GS (as an alternative to dual axis GSs) [18]; (iv) double prismatic PMs for generating short laser impulses; (v) double pyramidal PMs (a normal one inside a similar pyramidal cavity) for Optical Coherence Microscopy [19]; (vi) rotational pyramidal micro-mirrors for endoscope scanning probes for OCT [20].

Numerous studies on PM scanners exist. Practical equations to calculate the PM parameters have been developed [1, 2]. The off-set of a pre- or post-objective PM from the optical axis of its objective lens in order to obtain zero vignetting was determined [21]. Post-objective PMs were improved to achieve a flat field even without F-theta lenses [22], which is convenient due to cost issues, and even more for systems with high power lasers, taking into account the thermal effect. To unite different theories with the practical design, a vector approach was developed by Li, including PMs into a general theory of mirror-scanning devices; equations to characterize the scan field of a PM were obtained [23], as well as for 2D scanning [24]. In contrast to such general approaches and also to practical equations used to evaluate approximately the PM parameters [1], the scope of this study is to provide a rigorous, yet easy to use multi-parametric analysis of one of the most common PM scanning heads: with an off-axis PM and a collimated beam incident on the PM orthogonal to the optical axis (Fig. 1) of its objective lens [10, 11, 16]. The approach is not vectorial - as in previous studies [23, 24] – but purely geometrical and algebraic. The aim is to derive and study analytically the PM characteristic functions with regard to its constructive parameters. A classical aspect like the movement of the point of reflection on the PM facet leads to defining the migration functions.

Previous studies considered parallel beams with finite widths – for post-objective PMs [21], convergent beams – for pre-objective PMs [22], or just single rays through the system [23]. With the present theory the simple, convenient single ray approach can be used and then extended to take into account finite width beams. The study of vignetting and of the enlargement of the spots due to oblique incidence is thus made possible within the same theory. This analysis, for which several preliminary studies were performed [8, 25] allows for a better design of PM scanning heads for different systems, such as those mentioned above.

In the remaining of this paper, the theoretical study of the PM scanning heads is developed in Section 2, for each of its characteristic functions derived and studied. In Section 3 an experimental part validates the theoretical findings. In Section 4 design considerations of these setups are discussed from the analysis.

2. CHARACTERISTIC FUNCTIONS OF THE PM SCANNING HEADS

The main geometrical parameters of the setup are (Fig. 1): R, inner radius/apothem of the n facets PM; $\alpha = \pi/n$, angle corresponding to half a facet; e, eccentricity of the axis of the laser beam incident on the PM with regard to its pivot O; L, distance from this beam axis to the object principal plane of the lens, equal to its focal distance f; D, maximum scanned dimension, equal to the diameter of the entrance pupil of the lens. In the entire analysis only the ray incoming at distance e from the pivot O (i.e., the beam axis) is considered.

1. The scanning function $h(\theta)$ is defined as the distance from the optical axis (O.A.) of the objective lens of the PM to the axis of the scanning beam emerging this lens. This function is obtained from the construction in Fig. 1b, where a PM facet is considered in three positions: for $\theta = \theta_1$, $\pi/4$, and θ_2. These angles are measured considering $\theta = 0$ for the PM apothem on the vertical axis - when the PM facet is perpendicular on the y-axis; therefore θ_1 characterizes negative scans and θ_2 positive scans with regard to the neutral position $\theta = \pi/4$ [1, 11]. These are the rotational angles of the PM for which the margins of the useful scanned space (i.e., of the objective lens) are reached. The points P_1, M, and P_2 are the intersections of the incoming ray with the PM facet for the three rotation angles considered: θ_1, $\pi/4$, and θ_2, respectively.

In the Myz system of coordinates in Fig. 1b – where the origin M = P($\theta = \pi/4$), and P(y, z) is the current point of incidence of the ray on a PM facet – the scanning function is:

$$h(\theta) = y(\theta) - L/\tan 2\theta. \tag{1}$$

In order to obtain the coordinate y of the incidence point P, the equation of the facet on which the reflection is produced is considered in the O$\mu\zeta$ system of coordinates (Fig. 1b):

$$\zeta = \zeta_B + (\mu - \mu_B)\tan\theta \tag{2a}$$

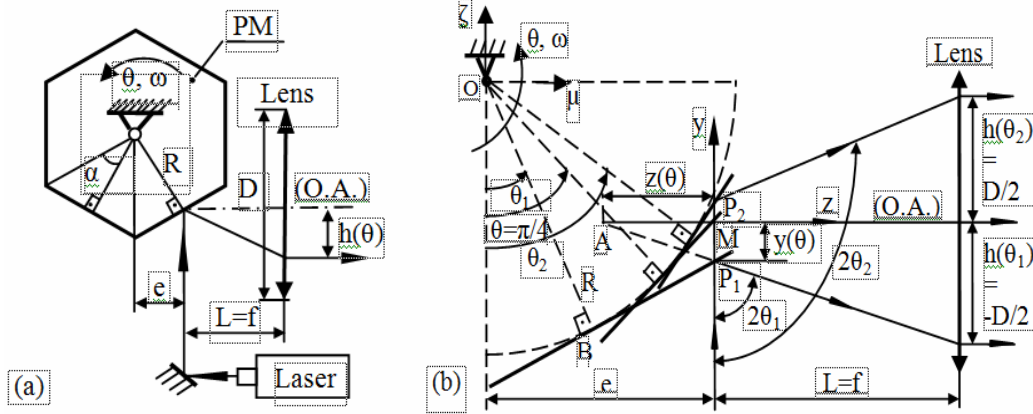$$\mu_B = R\sin\theta; \ \zeta_B = -R\cos\theta. \tag{2b}$$

Fig. 1 – a) Polygonal Mirror (PM) scanning head; b) PM facet in three characteristic positions: for $\theta = \theta_1$, $\pi/4$, and θ_2, where θ_1 and θ_2 are the angles for which the margins of the useful scanning domain, defined by the objective lens are reached; for $\theta = \pi/4$ the ray is reflected on the optical axis (O.A.) of the lens.

As M is the incidence point for the horizontal position of the reflected ray (for $\theta = \pi/4$), from Eq. (2)

$$\zeta_P = -R\cos\theta + (e - R\sin\theta)\tan\theta \tag{3a}$$
$$\zeta_M = e - R\sqrt{2}. \tag{3b}$$

Therefore, as $y = y_P - y_M$, using Eqs. (1) and (3), the expression of the scanning function is

$$h(\theta) = R\sqrt{2} - e - \frac{R}{\cos\theta} + e\cdot\tan\theta - \frac{L}{\tan 2\theta} \tag{4}$$

and its useful domain for the scanning process is the $[\theta_1, \theta_2]$ interval. Another pair of angles is also pointed out in Fig. 2: θ_{min} and θ_{max} represent the angles for which the scan of a facet starts and ends, respectively.

The issue of the $h(\theta)$ function is its non-linearity. For its linearization the three geometrical parameters in Eq. (4) (i.e., R, $\varepsilon = e/R$, and L) complicate the mathematical discussion, but they also allow for more degrees of freedom in the design with regard to the trivial case of the monogon/plane mirror scanner, rotating [25] or oscillatory [13–15]. When the number of PM facets n increases (e.g., for PM-based SSs for OCT), the angular scanning domain decreases, therefore the function $h(\theta)$ can be considered linear on portions.

2. The scanning velocity is, from Eq. (4), as $\omega = $ cst. (therefore $\theta = \omega t$),

$$v(t) = \frac{dh}{d\theta}\cdot\frac{d\theta}{dt} = \frac{\omega}{\cos^2\theta}\left[e - R\sin\theta + \frac{L}{2\sin^2\theta}\right]. \tag{5}$$

To achieve uni-directional scan, a no-return condition of the scanning ray must be fulfilled; this means $dh/d\theta > 0$, $(\forall)\theta \in [0, \pi/2]$. From Eq. (7) this condition is usually observed, since the distance $L=f$ is in most applications significantly larger than R (Fig. 1). However, for PMs with a larger n and therefore with a larger R (e.g., for PM-based SSs), L may be smaller than in optical micrometers for example [16], as more compact setups are used. In this case, as the angular scanning domains are also much smaller for larger n, one has $L > 2R\sin^3\theta$; therefore the no-return condition is also fulfilled in this situation.

Thus, as $h(\theta)$ is a continuously increasing function, $\theta = \pi/4$ is the only solution of the $h(\theta) = 0$ equation. The minimum value of the velocity, $v_{min} = v(\theta_m)$ is obtained for the angle θ_m that is the solution of the $dv/d\theta = 0$ equation; θ_m also provides the inflexion point of $h(\theta)$. One may see that this point is obtained for $\pi/4$ only if $e = 3R/2\sqrt{2}$, and in this case $v_{min} = 2\omega(e + L - R/\sqrt{2})$. However, in general,

$$dv/d\theta = 0 \quad => \quad Rs^5 - 2es^4 + Rs^3 - 2Ls^2 + L = 0, \tag{6}$$

with $s = \sin\theta$; therefore the graphic of „v" reaches its minimum for a slightly different angle (θ_m) than $\theta = \pi/4$ (Fig. 2b). For example, for a PM with $R = 15$ mm, $L = 100$ mm, and $e = 13.58$ mm (values to be considered for the experimental validations in Section 3), by solving numerically Eq. (6) the angle θ_m is 0.79128 rad. It can be demonstrated that Eq. (6) has a solution close to $\pi/4$ for any values of $R, L > 0$, and $e < 2R$.
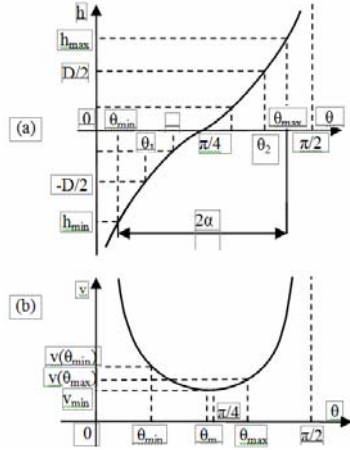
Fig. 2 – Scanning function (a) and scanning velocity (b) of the PM scanning head.
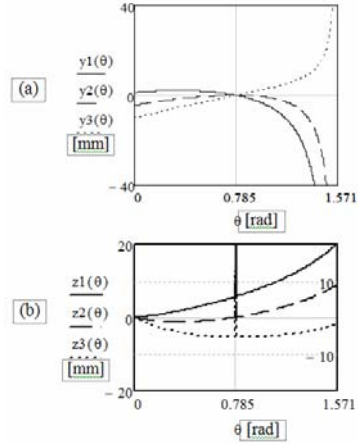
Fig. 3 – Transversal (a) and longitudinal (b) migration functions for $R = 15$ mm and $\varepsilon = e/R$ equals to: (1) 0.33; (2) 0.705; (3) 1.066.

Taking into account Eq. (5), the condition $\mathrm{d}^2h/\mathrm{d}\theta^2 \neq 0$, $(\forall)\theta \in [\theta_1, \theta_2]$ cannot be fulfilled, therefore $h(\theta)$ is always a non-linear function: the scan is thus always performed with a variable velocity over the entire domain (Fig. 2(b)), although in the vicinity of $\pi/4$ it can be considered constant for practical purposes – as $h(\theta)$ can be considered linear on that portion.

3. The migration functions characterize the phenomenon specific to PM scanning heads, i.e., the displacement of the incidence point P on a PM facet (Fig. 1b). This produces a „migration" of the object point A of the lens along the O.A., where the point A is defined by the intersection between the reflected ray and the O.A. It can be considered for the optical design of the objective lens of the PM that it is as if the ray incident on the lens was actually starting from A (Fig. 1(b)).

From Eqs. (1–4), *the transversal migration function* of the incidence point P (Fig. 1(b)) can be deduced as

$$y(\theta) = R\sqrt{2} - e - \frac{R}{\cos\theta} + e \cdot \tan\theta , \qquad (7)$$

while *the longitudinal migration function*, of the object point A along the O.A. is

$$z(\theta) = y(\theta)\tan 2\theta . \qquad (8)$$

The latter function is the most important for the design of such systems. It points out the method for the design of simpler lenses for the PM head: by correlating $z(\theta)$ with the spherical aberration $\mathrm{d}s_h$ of the lens. Thus, two important sources of errors of the system may compensate each other – at least in part. This can support the requirements of different scanners, to have the beam emerging the lens permanently parallel with the O.A. or to obtain a scan line into its focal plane – as required in most applications.

In Figs. 5 and 6 the migration functions $y(\theta)$ and $z(\theta)$ are studied with regard to the $\varepsilon = e/R$ factor, for its three characteristic cases: (1) $e < R(\sqrt{2} - 1)$; (2) $R(\sqrt{2} - 1) < e < R$; (3) $R < e < R\sqrt{2}$. A discussion on ε is necessary to obtain the case (thus, the graph) that is optimal for the PM setup – Section 4.

4. The scanning angles were pointed out in Fig. 1: θ_1 and θ_2, as well as θ_{min} and θ_{max}. The latter pair represents the rotational angles of the PM for which the scan of a facet begins, respectively ends; Beiser has introduced for them the terms of downdeflected and updeflected beams [1, 2]. From Fig. 4,

$$\begin{cases} \theta_{max} - \theta_{min} = 2\alpha \\ \sin(\theta_{min} + \alpha) = \dfrac{e\cos\alpha}{R} \end{cases} \implies \theta_{min,max} = \arcsin\frac{e \cdot \cos\alpha}{R} \mp \alpha . \qquad (9)$$

In consequence the angular scanning domain is:

$$\text{Total scan angle} = 2\theta_{max} - 2\theta_{min} = 4\alpha = 4\pi / n . \qquad (10)$$

In Figs. 5 and 6 the study of the two characteristic angles θ_{min} and θ_{max} is made with regard to the factor $\varepsilon = e/R$ (for $\alpha = \text{cst.}$) and with regard to the angle $\alpha = \pi/n$ (for the three different cases of ε considered in Fig. 5), respectively – based on Eq. (9). Several conclusions can be drawn from this discussion:

(i) From Fig. 5, for a certain α (i.e., for a given PM), the two angles are defined for a value of ε that may be chosen from $\tan\alpha$ to $1/\cos\alpha$. For $\varepsilon < \tan\alpha$, θ_{min} would be negative (the beam would be pointed opposite to Mz – Fig. 1). For ε closer to $1/\cos\alpha$, only a peak of the PM, i.e., a small portion of its facet would be used, and vignetting would become critical, therefore such values of ε should be avoided.

(ii) There is a constant difference of 2α between the two rotational angles – Eq. (9), and a 4α angle between the downdeflected and updeflected rays – Eq. (10). Therefore for PMs with few facets, as for dimensional measurements in industry, there is a large angular domain, for example $4\alpha = 144°$ for the usual pentagonal PM. This gives the possibility to measure significant linear dimensions with a PM-based optical micrometer [16]. For SSs this domain grows extremely narrow [9–12]: for $n = 24$, the total scanning domain 4α is $30°$; for $n = 72$, it decreases to $10°$; for the highest value in the literature, $n = 128$, it is just $5°37'30''$.

(iii) In Fig. 6, at a certain value of ε, the variation of the two angles with regard to α is studied for each specific interval of ε. For all the three cases the graphs of $\theta_{min}(\alpha)$ and $\theta_{max}(\alpha)$ can start only from $\alpha = \pi/n_{max}$, where n_{max} is the maximum number of facets that may be considered in order to accommodate a certain width of the beam for a minimum possible radius R. In this respect R should be increased, but one has to take into account that such an increase leads to multiple issues related to torque and mass (therefore to motor and bearings), to windage, structural integrity, and most of all to deformations of the facets at the high values of ω. The latter two issues impose a Finite Elements Analysis to be carried out for each PM configuration [1].

(iv) For the graphs in Fig. 6 the maximum value of α is $\pi/3$, although in practice at least square PMs are used, therefore the practical limit is $\alpha_{max} = \pi/4$. For $\alpha = \pi/3$ a limit value of ε is obtained: from $\mathrm{atan}(x) = \pi/3$, $e = R\sqrt{3}$; thus $1 < \varepsilon < \sqrt{3}$. This limit situation should be avoided because of vignetting, as pointed out at (i).

5. The duty cycle, defined as the ratio between the time used for the scanning process and the total time interval, is with Eq. (9) and taking into account that the rotational speed of the mirror $\omega = $ cst.
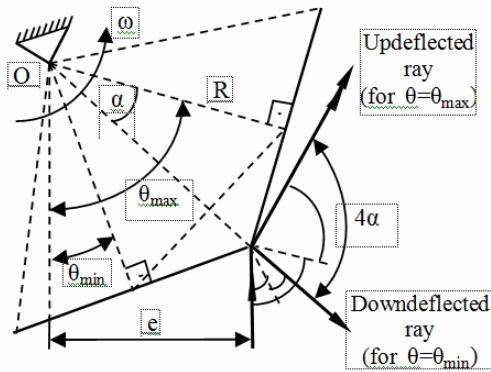

Fig. 4 – The rotational angles of the PM, θ_{min} and θ_{max} for which the ray reaches the margins of a PM facet.
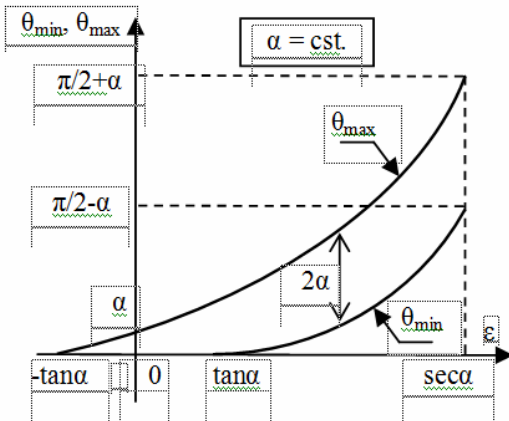

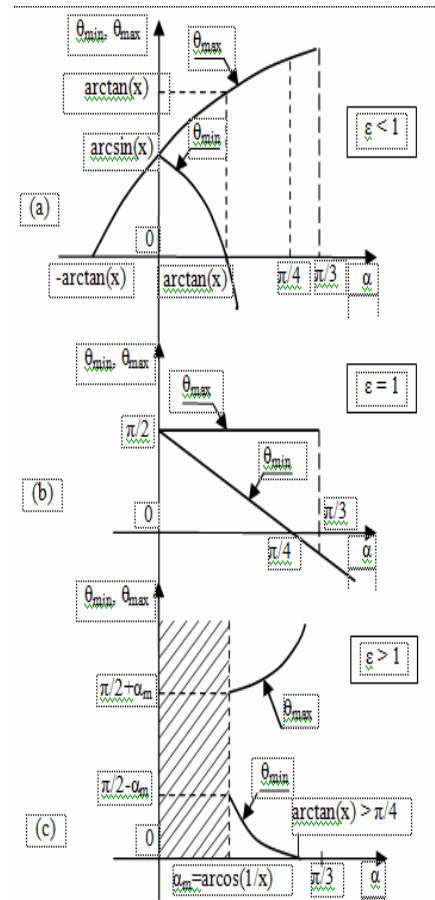Fig. 5 – Characteristic angles studied with regard to $\varepsilon = e/R$.

Fig. 6 – Characteristics angles studied with regard to $\alpha = \pi/n$.

$$\eta = \frac{2(\theta_2 - \theta_1)}{2(\theta_{max} - \theta_{min})} = n\frac{\theta_2 - \theta_1}{2\pi}$$

This duty cycle characterizes the entire scanning head. By contrast, the duty cycle defined in the literature [1, 2] often takes into account only the vignetting on a PM facet, therefore characterizes only the polygon. Also, from Eq. (11), at the same values of θ_1 and θ_2, the duty cycle is n times higher for the PM than for the monogon scanner [25]. A discussion on η is necessary for the designing calculus of the device:

$$\text{(i) } \eta < 1 \qquad \Leftrightarrow \qquad \theta_{min} < \theta_1 < \theta_2 < \theta_{max}. \tag{12}$$

In this case the entire diameter D of the lens in the meridian plane Myz (Fig. 1) is scanned by the rotating beam. Therefore the lens is positioned inside the total scanning domain defined by the positions of the rays produced at the θ_{min} and θ_{max} rotational angles (Fig. 4): the extreme rays given by the θ_1 and θ_2 angles of the useful scanning domain can thus be placed simmetrically with regard to a horizontal axis, which is the O.A.

$$\text{(ii) } \eta = 1 \qquad \Leftrightarrow \qquad \theta_{min} = \theta_1 \quad \text{and} \quad \theta_2 = \theta_{max}. \tag{13}$$

This is a condition difficult to match in practice. It means that the O.A. is no more perpendicular to the ray incident on the PM. This happens because the total angular scanning domain is in general asymmetric with regard to the horizontal axis (Fig. 4). The particular symmetry case could be achieved only for:

$$\pi/2 - 2\theta_{min} = 2\alpha \implies e = R/\sqrt{2}\cos\alpha. \tag{14}$$

$$\text{(iii) } \eta > 1 \qquad \Leftrightarrow \qquad \theta_1 < \theta_{min} < \theta_{max} < \theta_2. \tag{15}$$

This case, for which the lens is larger than the scanning domain corresponds to PMs with a large n – as for SSs. From Fig. 6, for a small angle α, the scanning domain 4α narrows, as exemplified in the previous subsection. However, in practice $\eta > 1$ is achieved only for double-pass PMs [1, 2] – for which the scan on the next facet begins before the scan on the current facet is completed; to achieve this, the incoming beam is split in two. If that is not the case, than the Eq. (11) of the duty cycle is valid only for $\eta \le 1$.

3. EXPERIMENTAL STUDY

The experimental setup in Fig. 7a consists of a laser, a translational stage on which scanning heads with different PMs can be mounted, and a photo-detector (PD) placed on another translational stage to measure the current position of the reflected beam on the line Δ that represents the object principal plane of the objective lens in Fig. 1. With the translation stage on which the PM is placed one can adjust the distance L between the fix laser ray and the line Δ, as well as the eccentricity e.

The scanning functions can thus be studied with regard to the constructive parameters of the device. An example obtained for n equals 5 is presented in Fig. 7b to illustrate the experimental analysis presented in the following. The issue of these experiments is that the measured displacement x of the laser spot differs from h, and the measured angle ψ differs from θ – as the experimental system of coordinates was chosen differently from the one considered in the theoretical study (Fig. 7a).

To compare the experimental and theoretical data, a necessary change of coordinates has to be done. The steps to obtain the scanning function $h(\theta)$ from the experimental data $x(\Psi)$ are – as shown in the example in Table 1 for a pentagonal PM: (i) the angles θ_{min} and θ_{max}, Eq. (9) are calculated; (ii) the corresponding angles ψ_{min} and ψ_{max} for which the scan of a facet begins, respectively ends are determined, with a difference between them which results $72° = 2\alpha = \theta_{max} - \theta_{min}$, verifying Eq. (9); (iii) the corresponding angles ψ_{min} and θ_{min}, respectively ψ_{max} and θ_{max} are set in coincidence; (iv) the angle ψ for which θ equals 45°, therefore $h = 0$ is determined: $\psi(\theta = 45°) = 96°$; (v) the experimental scanning function is obtained, as $h_{exp}(\theta) = x(\theta) - x(\theta = 45°)$; (vi) the calculated and experimental functions are compared, and from Fig. 7(b), a good match is obtained.

From these graphs of $h_{calc}(\theta)$ and $h_{exp}(\theta)$ in Fig. 7b a slight non-linearity is remarked at the margins of the scanned domain; this can be eliminated by using appropriate scan lenses [1]. To capture the entire

domain and thus to visualize the full profile of $h(\theta)$, with its strong non-linearity, in Fig. 7c, the measuring line was positioned much closer, at $L = 18$ mm – to obtain the translated graph $x(\psi)$. A qualitative match is thus obtained with the theoretical graph of $h(\theta)$ in Fig. 2a. In conclusion, the most efficient method to obtain a more linear function $h(\theta)$ is the increase of L – as for monogon scanners [25]). On the other hand, for a given L, the maximum angular domain $[\theta_1, \theta_2]$ can be chosen to keep the non-linearity of the function $h(\theta)$ bellow a certain ratio – to use the PM even without a scan lens, as in telescope-less SSs [11, 12].

Table 1

The correlation of the experimental results with the theory

θ [°]	$\theta_{min} = 11$	27	45	63	$\theta_{max} = 83$
Ψ [°]	$\Psi(\theta_{min}) = 62$	78	96	134	$\Psi(\theta_{max}) = 134$
x [mm]	–	– 46	146	330	
h_{exp} [mm]	–	– 192	0	184	–
h_{calc} [mm]	– 668.32	– 196.98	0	195.93	1069.86

In this latter case one uses a part of the graph much smaller than the one of the entire scan domain $h(\theta) = h(\theta_{max}) - h(\theta_{min})$, which is large – for example 1738.18 mm for the pentagonal PM in Fig. 7b, for $L = 100$ mm. A final discussion in this experimental part should be made on the ascertainment of $h(\theta)$ for different values of the eccentricity e (Fig. 7a). Thus e should be chosen with regard to R to have – Eq. (9) – the angle $\theta_{min} > 0$, in order to allow for using the entire scan domain (otherwise part of the reflected beams would be directed opposite to the Mz-axis). This aspect is discussed in the following.
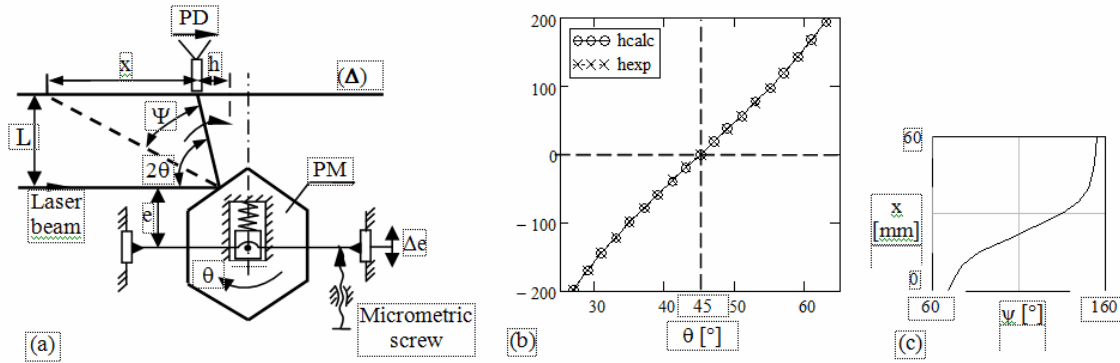

Fig. 7a – Setup for the study of PM scanning heads - principle scheme; b) theoretical versus experimental scanning function of the PM for $n = 5$, with $L = 100$ mm and $e = 13.58$ mm; c) experimental scanning function (translated, $x(\psi)$ measured function) for the same value of e and a small distance $L = 18$ mm – to capture the entire graph of the scanning function.

4. DISCUSSION ON THE DESIGN OF PM SCANNING HEADS

From the geometry in Fig. 1, the following conditions must be preserved: $\theta_1 > 0$, $\theta_2 < \pi/2$, and $\theta_{min} < \pi/4 < \theta_{max}$. From the first two conditions the entire scanning domain is available to position the lens, while from the latter one the scanned space is situated on both sides of the lens axis. From these conditions, using Eq. (9), several relationships of the constructive parameters of the scanning system can be obtained:

$$0 < \theta_{min} < \theta_1 < \pi/4 < \theta_{max} < \theta_2 < \pi/2 \quad => \quad \left| 1 - \frac{e\sqrt{2}}{R} \right| < \tan\alpha < \frac{e}{R} < 1 \tag{16}$$

The following consequences are thus obtained for the design of PM scanning heads:

(i) The transversal migration function $y(\theta)$, Eq. (5), is characterized by the graph obtained for $\sqrt{2} - 1 < \varepsilon < 1$, $\varepsilon = e/R$ (Fig. 3a). The other two cases of the $y(\theta)$ function are not to be used for this scanner configuration.

(ii) The longitudinal migration function $z(\theta)$, Eq. (6), is characterized by the graph for the same case.

(iii) The $\varepsilon < 1$ case is valid for the angles θ_{min} and θ_{max} studied with regard to the angle α (Fig. 6a). (iv) Considering only the conditions $\theta_{min} > 0$ and $\theta_{max} < \pi/2$, necessary in order to increase the duty cycle, with Eq. (9) one obtains $n \geq 5$, therefore at least a pentagon PM has to be used in this scanner configuration.

As this analysis uses collimated laser beams, it also allows one to consider the finite width of the beam by taking into account slight variations of the eccentricity e of the fix incident beam. This allows one to obtain the variations of the dimensions of the reflected beam due to the scan aperture, and also to approach the vignetting issues at the facet edges, essential especially for a high n, as in PM-based SSs for OCT. Another direction of work opened by this study refers to the correlation of the migration functions deduced with the spherical aberration of the lens for the compensation of these two major sources of errors into the system.

5. CONCLUSIONS

The study performed a multi-parameter analysis of the characteristic functions of PM scanning heads for collimated laser beams incident on the PM, including: the scanning function and velocity, the characteristic pairs of angles of the process, the duty cycle, and the migration functions generated by the non-stationary intersection between the incident ray and the eccentric rotational PM facet. These functions were deduced and studied with regard to the constructive parameters of the device: dimension and number of PM facets, position of the fix incident beam with regard to the PM pivot and to its objective lens, and rotational speed of the PM. An experimental validation of the theory was completed. Design rules-of-thumb to optimize PM scanning heads were extracted from the analysis. On-going applications in our group include different PM-based SSs applied in a range of OCT applications, from biomedical imaging to non-destructive testing.

ACKNOWLEDGEMENTS

REFERENCES

1. G.F. MARSHALL, G.E. STUTZ, Eds., *Handbook of optical and laser scanning*, CRC Press, London, 2011.
2. M. BASS, Ed., *Handbook of optics*, 3rd Edition, Mc. Graw-Hill Inc., New York, 2009, pp. 30.1–30.68.
3. D. HUANG *et al*., *Optical coherence tomography*, Science, **254**, pp. 1178–1181, 1991.
4. W. DREXLER, M. LIU, A. KUMAR, T. KAMALI, A. UNTERHUBER, R.A. LEITGEB, *Optical coherence tomography today: speed, contrast, and multimodality*, J. Biomed. Opt., **19**, 071412, 2014.
5. A.G. PODOLEANU, R.B. ROSEN, *Combinations of techniques in imaging the retina with high resolution*, Progress in Retinal and Eye Research, **27**, pp. 464–499, 2008.
6. D.C. ADLER, Y. CHEN, R. HUBER, J. SCHMITT, J. CONNOLLY, J.G. FUJIMOTO, *Three-dimensional endomicroscopy using optical coherence tomography*, Nature Photonics, **1**, pp. 709–716, 2007.
7. J. MONTAGU, *Scanners-galvanometric and resonant*, Encyclopedia of Opt. Eng., Taylor & Francis, 2003, pp. 2465–2487.
8. V.-F. DUMA, J.P. ROLLAND, A.G. PODOLEANU, *Perspectives of optical scanning in OCT*, Proc SPIE **7556**, 7556–10, 2010.
9. S.H. YUN, C. BOUDOUX, G.J. TEARNEY, B.E. BOUMA, *High-speed wavelength-swept semiconductor laser with a polygon-scanner-based wavelength filter*, Opt. Letters, **28**, pp. 1981–1983, 2003.
10. W.Y. OH, S.H. YUN, G.J. TEARNEY, B.E. BOUMA, *115 kHz tuning repetition rate ultrahigh-speed wavelength-swept semiconductor laser*, Opt. Letters, **30**, pp. 3159–3161, 2005.
11. S.M.R. MOTAGHIAN NEZAM, *High-speed polygon-scanner-based wavelength-swept laser source in the telescope-less configurations with application in optical coherence tomography*, Opt. Letters, **33**, pp. 1741–1743, 2008.
12. M.K.K. LEUNG *et al.*, *High-power wavelength-swept laser in Littman telescope-less polygon filter and dual-amplifier configuration for multichannel optical coherence tomography*, Opt. Letters, **34**, pp. 2814–2816, 2009.
13. V.-F. DUMA, *Optimal scanning function of a galvanometer scanner for an increased duty cycle*, Opt. Eng., **49**, 103001, 2010.
14. V.-F. DUMA, K.-S. LEE, P. MEEMON, J.P. ROLLAND, *Experimental investigations of the scanning functions of galvanometer-based scanners with applications in OCT*, Appl. Opt., **50**, pp. 5735–5749, 2011.
15. V.-F. DUMA, P. TANKAM, J. HUANG, J.J. WON, J.P. ROLLAND, *Optimization of galvanometer scanning for Optical Coherence Tomography,* Appl. Opt., **54**, pp. 5495–5507, 2015.

16. B. RICHTER, *Laser scan devices for industrial application*, WIRE, **42**, pp. 529–541, 1992.
17. A.L. OLDENBURG, J.J. REYNOLDS, D.L. MARKS, S.A. BOPPART, *Fast-Fourier-domain delay line for in vivo optical coherence tomography with a polygonal scanner*, Appl. Opt., **42**, pp. 4606–4611, 2003.
18. K. H. KIM, C. BUEHLER, P.T.C. SO, *High-speed, two-photon scanning microscope*, Appl. Opt., **38**, pp. 6004–6009, 1999.
19. L. LIU *et al.*, *Double-reflection polygon mirror for high-speed optical coherence microscopy*, Opt. Letters, **32**, pp. 3528–3530, 2007.
20. X. MU, G. ZHOU, H. YU, Y. DU, H. FENG, J.M.L. TSAI, F.S. CHAU, *Compact MEMS-driven pyramidal polygon reflector for circumferential scanned endoscopic imaging probe*, Opt. Express, **20**, pp. 6325–6339, 2012.
21. K.O.G. VARUGHESE, K. SIVA RAMA KRISHNA, *Flattening the field of postobjective scanners by optimum choice and positioning of polygons*, Appl. Opt., **32**, pp. 1104–1108, 1993.
22. C.T. WALTERS, *Flat-field postobjective polygon scanner*, Appl. Opt., **34**, pp. 2220–2225, 1995.
23. Y. LI, J. KATZ, *Asymmetric distribution of the scanned field of a rotating reflective polygon*, Appl. Opt., **36**, pp. 342–352, 1997.
24. Y. LI, *Beam deflection and scanning by two-mirror and two-axis systems of different architectures: a unified approach*, Appl. Opt., **47**, pp. 5976–5985, 2008.
25. V.-F. DUMA, *Novel approaches in the design of polygon scanners*, Proc. SPIE, **6785**, 6785-1Q, 2007.